Theoretical modeling of the complexes of iron impurities and oxygen vacancies in $SrTiO_3$

Evgeny Blokhin,[1,a)] Eugene Kotomin,[1,2] Alexei Kuzmin,[2] Juris Purans,[2] Robert Evarestov,[3] and Joachim Maier[1]
[1]*Max-Planck Institute for Solid State Research, Stuttgart, Germany*
[2]*Institute for Solid State Physics, University of Latvia, Riga, Latvia*
[3]*Department of Quantum Chemistry, St. Petersburg State University, Peterhof, Russia*

(Received 18 February 2013; accepted 8 March 2013; published online 21 March 2013)

The combined use of *ab initio* quantum mechanical and x-ray absorption near edge structure (XANES) methods confirms that the oxygen vacancies (V_O) are located in the first coordination shell of Fe^{3+} ions in the cathodic region of electrocolored Fe^{3+}-doped $SrTiO_3$. The binding energy of such a complex is estimated as ~0.4 eV. The lattice distortions obtained in *ab initio* modeling and extended x-ray absorption fine structure experiments are in agreement. The predicted distortions make a minor effect on a simulated XANES signal, and its shape mainly depends on the presence of V_O in the Fe^{3+} first coordination shell. Additionally, formation of the Fe^{3+}–V_O complex leads to disappearance of the phonon frequencies in the range of 620–760 cm^{-1} of the calculated phonon spectrum. © *2013 American Institute of Physics*. [http://dx.doi.org/10.1063/1.4796182]

Fe-doped $SrTiO_3$ became a model material for a wide class of mixed electronic-ionic conductors. Oxygen vacancies (V_O) and iron impurities in $SrTiO_3$, as well as their complexes, play a key role in electrooptical applications and non-volatile resistive random access switching memories.[1] For example, the understanding of the relative spatial distribution of Fe ions and V_O is important to explain the formation of the conductive filaments.[2] Recently Fe impurities (substituting B-type cations) and V_O in $SrTiO_3$—separated[3–5] and associated[6–12]—have been addressed by a number of approaches. It has been shown by the electron paramagnetic resonance technique that there is a perceptible attraction between iron impurity and V_O yielding $Fe^{3+}-V_O$ complexes even at dopant concentration below 0.1 at. % while such defect pairs are completely dissociated at temperatures above 300 °C.[6] Also, the Jahn-Teller (JT) distortion around iron impurities and V_O defects was studied. In particular, this effect has been fingerprinted by the appearance of the observable Raman modes in the $SrTiO_3$ phonon spectra[5,12] in the range of 620–760 cm^{-1}.

In this letter, we study the effect of iron impurity and V_O interactions in the first and more distant coordination shells in $SrTiO_3$, in order to interpret the recent x-ray absorption near edge structure (XANES) experiments on resistive switching structures[9,10] and predict the relevant phonon spectra.

The *ab initio* spin-polarized calculations of the ground-state atomic structures were performed with the CRYSTAL09 computer code.[13] A supercell approach[14] was used to consider the defects in $SrTiO_3$ host matrix. To this end, we have chosen the 80-atom supercell (expansion matrix [0 2 2; 2 0 2; 2 2 0]). The phonon frequencies for the relaxed ground-state defective structures were calculated by the frozen phonon method (harmonic approximation). We used a basis set (BS) of linear combination of atomic orbitals (LCAO) and PBE0 (Ref. 15) hybrid exchange-correlation DFT functional. For Ti and Sr atoms we adopted the small-core effective core potentials (ECP)[16] whereas for Fe and O atoms the all-electron basis sets[17] were used. The level of numerical approximation in evaluating the Coulomb and exchange series appearing in the self-consistent field equations for periodic systems was controlled by five tolerances: 10^{-8}, 10^{-8}, 10^{-8}, 10^{-8}, and 10^{-16} (related to estimates of overlap or penetration for integrals of Gaussian functions on different centers, which define cutoff limits for series summation). The reciprocal space was sampled according to a regular sublattice defined by $8 \times 8 \times 8$ k-points in the irreducible Brillouin zone (BZ) of a perfect $SrTiO_3$, being accordingly 64 times reduced for the 80-atom supercell. The tolerance of the energy convergence on the self-consistent field (SCF) cycles was set to 10^{-8} a.u for the full structure relaxation and 10^{-10} a.u. for the phonon frequencies calculation. The DFT density and grid weight tolerances were increased (8 and 16 in CRYSTAL09), and an extra-large pruned DFT integration grid was adopted. In all the calculations neutral supercells were used. In particular, the electronic density of a missing O ion was allowed to redistribute between the vacancy and the nearest ions[5] in order to get the minimal total energy. As a result, the V_O retains relatively small electron density and could be considered as a charged defect.

This computational set was previously shown to very well reproduce the known structural, electronic, and phonon properties of ideal $SrTiO_3$,[18] as well as defective $SrTiO_3$ containing Fe and V_O separately.[5] Here we applied it to the four structural models schematically shown in Fig. 1.

The model 1 corresponds to Fe^{4+} impurity which shows the JT distortion[3,4] of the local environment without oxygen vacancies. The models 2–4 contain one V_O and two Fe atoms per supercell, thus forming a neutral defect complex (following the formal ionic charges Sr^{2+}, Ti^{4+}, O^{2-}, Fe^{3+}). Calculated Fe magnetic moments (3.6 μ_B for Fe^{4+} in model 1 and 4.3 μ_B for Fe^{3+} in models 2–4) follow the Hund rule of high spin on Fe ions and confirm partial covalency of the chemical bonding in $SrTiO_3$.

a)Author to whom correspondence should be addressed. Electronic mail: e.blokhin@fkf.mpg.de.

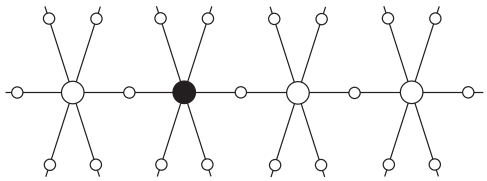

model 1

Fe^{4+}

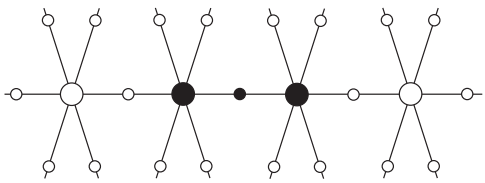

model 2

$Fe^{3+}–V_O–Fe^{3+}$

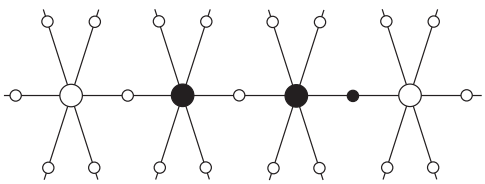

model 3

$Fe^{3+}–O–Fe^{3+}–V_O$

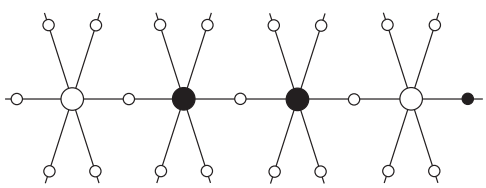

model 4

$Fe^{3+}–O–Fe^{3+}–O–Ti–V_O$

FIG. 1. Schematic view of the four structural models (Ti — ○, O — ○, Fe — ●, V_O — ●).

Experimentally it is not known how Fe and V_O are *de facto* distributed across the $SrTiO_3$ matrix since the extended x-ray absorption fine structure (EXAFS) technique[9] can only distinguish the atomic coordination shells of Fe ions. Therefore, the following cases were considered: model 2 with V_O in the first coordinaton shell of two Fe ions, model 3 with V_O in different coordination shells of two (thus nonequivalent) Fe ions, and model 4 with V_O and Fe maximally separated from each other within a supercell. After relaxation the oxygen atoms near each iron impurity are grouped into *planar* (four O_{pl} belonging to the same plane) and *axial* (remaining two or one O_{ax}, depending on V_O presence nearby Fe).

The defect formation energies (E_{form}) were calculated using the following relation:

$$E_{form} = E_{tot.el}(SrTi_{1-x}Fe_xO_{3-\delta}) - n\,E_{tot.el}(\text{Fe atom}) + n\,E_{tot.el}(\text{Ti atom}) + m\,E_{tot.el}(\text{O atom}) - N\,E_{tot.el}(SrTiO_3), \quad (1)$$

where n and m are the numbers of iron impurities and oxygen vacancies, considered in a model, N is the number of primitive $SrTiO_3$ unit cells in the supercell (16), x is n/N, and δ is m/N.

X-ray absorption spectroscopy is a local structural tool perfectly suited for investigation of relaxation effects around impurity atoms in crystalline and disordered compounds.[19] However, the analysis of XANES is a complicated task due to a contribution of high-order multiple-scattering processes,[20,21] which reflect many-atom distribution functions or the 3D atomic structure. The XANES spectrum of a crystalline compound is usually calculated for a static equilibrium atomic structure, typically known from a diffraction experiment, while a configurational average is required to achieve good agreement between theoretical and experimental XANES signals.[21]

In the case of impurity atoms, the relaxation of their local environment must be taken into account in the XANES calculations. Since the effect of relaxation is usually not known a priori and cannot be determined experimentally by other techniques with the required accuracy (about 0.01 Å or better), one needs to search for an alternative solution. The answer can be found in the combined use of *ab initio* quantum mechanical and XANES methods. Such an approach allows one to couple the results of two theoretical methods by computing XANES spectrum for the *ab initio* calculated ground-state atomic structure. The agreement between theoretical and experimental XANES spectra can be used as an estimate of the accuracy of the structure relaxation determined by the *ab initio* calculation.

In this study self-consistent, real-space full-multiple-scattering XANES calculations of the Fe K-edge in Fe-doped $SrTiO_3$ were performed by the FDMNES code[22,23] in the one-electron electric dipole ($\Delta l = 1$, $1s \rightarrow np$) and quadrupole ($\Delta l = 2$, $1s \rightarrow nd$) approximations for the four structural models shown in Fig. 1. The self-consistent cluster potential was calculated within the non-muffin-tin approximation using the finite difference method (FDM),[22] in which the full cluster potential is set on an equally spaced 3D-grid. The radius of all clusters was equal to 6.0 Å, being sufficiently large to reproduce the main features in the experimental Fe K-edge XANES signal. The real Hedin-Lundqvist exchange-correlation potential[24] was employed in the calculations, and the final excited state of the photoelectron included a screened core-hole. Thus, the calculated Fe K-edge XANES spectra were intentionally not broadened to underline the details of the fine structure.

The experimental Fe K-edge XANES spectrum for the cathodic region of the electrocolored Fe^{3+}-doped $SrTiO_3$ single crystal has been discussed in Ref. 9. The four distinctive features (A, B, C, D) can be observed in the experimental XANES spectrum below the main absorption edge E (Fig. 2). In the dipole approximation, the $1s$ (Fe) core-electron is excited into unoccupied final-states with p-character. Such transitions are the origin of all the peaks above A. The transition of the $1s$ (Fe) electron to the conduction band of

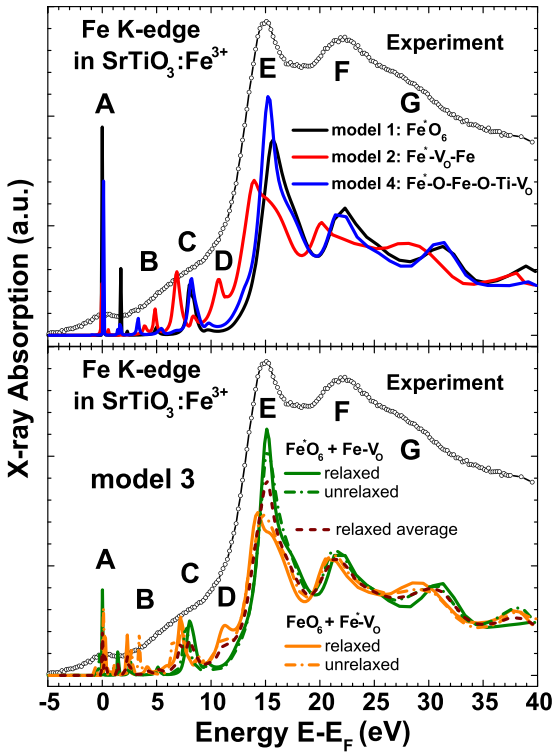

FIG. 2. Comparison of the experimental[9] and calculated (models 1–4) Fe K-edge XANES spectra. For the model 3 the XANES spectra for the two relaxed (unrelaxed) Fe sites are shown by solid (dashed-dotted) lines, and the average XANES spectrum for relaxed structure is shown by dashed line. The zero of energy scale corresponds to the theoretical Fermi level E_F.

Fe-doped $SrTiO_3$ (peak A in Fig. 2) is forbidden in the dipole approximation since the band is composed mainly of the 3*d*-metal ion (Ti/Fe) states. However, such a transition can become allowed either (i) within the quadrupole approximation or (ii) due to the lowering of local symmetry, caused by the JT distortion[3,4] or by the presence of the V_O in the first coordination shell of the iron atom.

In the model 1, four short Fe−O distances of about 1.88 Å and two long Fe−O distances of about 2.07 Å (Table I) were obtained from *ab initio* calculations as a result of the JT distortion. Such a structural model is able to reproduce the main peaks observed in the experimental Fe K-edge XANES but fails to predict the absorption in the region of the peaks D and G.

In the model 2, a single oxygen vacancy is placed between two iron atoms so that they become five-fold coordinated. The mutual Coulomb repulsion causes the shifts of the two iron ions in opposite directions (by 0.14 Å each). The planar oxygen atoms move by 0.11 Å towards the V_O and by 0.02 Å away the iron ions: thus, four Fe−O distances become 1.98 Å, in good agreement with the EXAFS results[9] (Table I). The peculiar aspect of this model is the appearance of the peak D in the Fe K-edge XANES signal, the decrease of the peak E intensity, and a shift of all peak positions to smaller energies. This model also predicts a shift of the peak G at 31 eV down to ~28 eV, which explains the origin of the shoulder in the experimental data. To conclude, this model gives good overall agreement with the experimental XANES spectrum.

In the model 4, a single oxygen vacancy is placed in the third coordinaton shell of Fe^{3+} ions. In this case, two Ti atoms near V_O are repelled in opposite directions (by 0.18 Å each). Six oxygen atoms around the iron ions also relax considerably (Table I). The average Fe−O distance (2.00 Å) is larger than for models 1 and 2, following the EXAFS results.[9] Note that in $LaFeO_3$ (which can be considered as a reference system for a Fe^{3+} state) we have obtained an average distance Fe–O as 2.01 Å (orthorhombic phase), exactly corresponding to the experimental value.[25] The Fe K-edge XANES signal for the model 4 has the least agreement with the experiment: the peak D is completely absent, and the main peak E becomes more intense.

Lastly, the special feature of the model 3 is that the two Fe^{3+} ions occupy nonequivalent sites, which represent an intermediate situation between models 2 and 4. Therefore the total Fe K-edge XANES signal for the model 3 is computed as the average of those for the two iron sites. In Fig. 2 we show the XANES signals for both the five-fold and six-fold

TABLE I. Comparison of the models by the total electronic energy and structural distortions, obtained from *ab initio* simulations (Ti–O distance in a pure $SrTiO_3$ is 1.96 Å).

Model	Defects formation energy, E_{form} (eV)		Interatomic distances (Å)		
			ab initio Fe–$O_{pl.}$ Fe–$O_{ax.}$	*ab initio* Fe–O averaged	EXAFS[9] Fe–O averaged
1. Fe^{4+}	2.22	Fe_1	4 × 1.88 2 × 2.07	1.94	1.93
2. Fe^{3+}–V_O–Fe^{3+}	9.13	$Fe_{1,2}$	4 × 1.98 1 × 1.85	1.95	1.96
3. Fe^{3+}–O–Fe^{3+}–V_O	9.35	Fe_1	4 × 2.01 1 × 1.93, 1 × 2.00	2.00	1.97
		Fe_2	4 × 1.98 1 × 1.83	1.95	1.96
4. Fe^{3+}–O–Fe^{3+}–O–Ti–V_O	9.50	$Fe_{1,2}$	4 × 2.01 1 × 1.90, 1 × 2.05	2.00	1.97
$LaFeO_3$	...		2 × 2.00, 4 × 2.01	2.01	2.01[a]

[a]Neutron diffraction experiments[25] below 298 K.

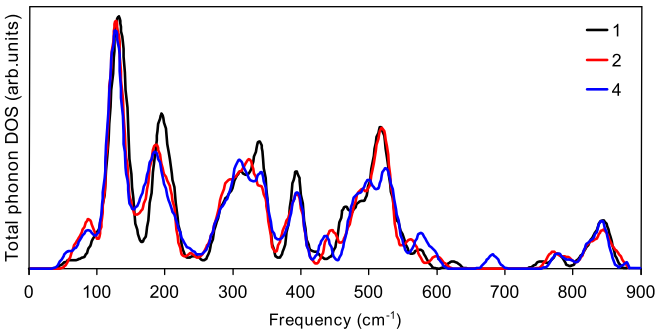

FIG. 3. The calculated total phonon DOS for the models 1, 2, and 4. The phonon frequencies were smeared according to a normal distribution (smearing width 10 cm^{-1}). Note the range of 620–760 cm^{-1}.

coordinated Fe in unrelaxed and relaxed environments as well as the average XANES signal for the relaxed structure. Note that the average XANES signal gives the *best* agreement with the experiment: the shoulder D is present, the peak G resides near 30 eV, and the shape of peak E agrees with the experimental one.

The model 3 shows also that the *ab initio* lattice relaxation produces a small effect on the shape of the XANES signal. The impact of relaxation is similar for other models. A comparison of the averaged atomic distortions around each of the two nonequivalent Fe^{3+} ions (Table I) shows a less pronounced relaxation near V_O and a more pronounced away from V_O. This difference agrees with the EXAFS results[9] and is mainly due to planar oxygen atoms.

Note that the presence of V_O in the nearest shell of Fe^{3+} determines the relaxation pattern. In all the models 2–4, the Fe ion near V_O moves outward by ~0.10 Å while the Fe ion far from V_O experiences practically no displacement (this can be seen in the change of the distance Fe–O_{ax}). The redistribution of the electron density from V_O to the nearest *d*-metal cations leads to the competition of Coulomb attraction and repulsion effects, resulting in the residual repulsion between iron impurities and planar O atoms. This long-range effect is traced in the EXAFS experiment.

A comparison of the defect formation energies for the models 2 and 4 allows us to estimate the binding energy between Fe^{3+} and V_O in the first coordination shell to be ~0.4 eV (in good agreement with the experimental estimate of 0.3 eV (Ref. 6) and the results of atomistic simulations[26]), i.e., the Fe^{3+}–V_O pairs are stable at around room temperature.

The phonon densities of states (DOS) for a perfect $SrTiO_3$ as well as for single Fe^{4+} and V_O point defects have been reported earlier.[5] Our calculations have shown that both defects are responsible for the new phonon modes in the range of 620–760 cm^{-1}. Fig. 3 shows the phonon DOS for models 1, 2, and 4. One can see that formation of the Fe^{3+}–V_O complex (model 2) leads to the disappearance of the phonon modes in the range of 620–760 cm^{-1} while for all other models (including model 3) this range is non-empty. This agrees with the recent Raman and IR spectroscopy results,[9,12] where no significant phonon intensity was observed in this range for the Fe^{3+} case, in contrast to the Fe^{4+} case. Note that the calculated DOS represents a semiquantitative picture since only the Γ point frequencies can be used.

To conclude, we performed *ab initio* DFT LCAO calculations with hybrid PBE0 functional of the lattice relaxation for different Fe^{3+}–V_O complexes in Fe^{3+}-doped $SrTiO_3$ and used them to simulate the Fe K-edge XANES spectra, which are compared to the experimental data for the cathodic region of electrocolored samples. The obtained results suggest that the presence of the oxygen vacancy in the *first* coordination shell of iron is crucial for the qualitative interpretation of the experimental XANES signal while the *ab initio* lattice relaxation effects are less important. On the other hand, the lattice relaxations obtained for different complexes are in good agreement with the EXAFS experiments. In the calculated phonon spectra, the Fe^{3+}–V_O complex formation is manifested by the absence of the phonon frequencies near 700 cm^{-1}, in agreement with the recent Raman and IR spectroscopy results.

Authors are greatly indebted to R. Merkle, R. Dittmann, and A.-M. Koehl for the discussions. This research was partly supported by the Latvian ERAF Project No. 2010/0272/2DP/2.1.1.1.0/10/APIA/VIAA/088 and Jülich Supercomputing Centre (Project HSS13).

[1]H. Donnerberg, *Atomic Simulations of Electrooptic and Magnetooptic Oxide Materials*, Springer Tracts in Modern Physics Vol. 151 (Springer, New York, 1999).
[2]R. Waser and M. Aono, Nature Mater. **6**, 833 (2007).
[3]R. A. Evarestov, S. Piskunov, E. A. Kotomin, and G. Borstel, Phys. Rev. B **67**, 064101 (2003).
[4]V. E. Alexandrov, J. Maier, and R. A. Evarestov, Phys. Rev. B **77**, 075111 (2008).
[5]R. A. Evarestov, E. Blokhin, D. Gryaznov, E. A. Kotomin, R. Merkle, and J. Maier, Phys. Rev. B **85**, 174303 (2012).
[6]R. Merkle and J. Maier, Phys. Chem. Chem. Phys. **5**, 2297 (2003).
[7]K. Szot, W. Speier, G. Bihlmayer, and R. Waser, Nature Mater. **5**, 312 (2006).
[8]R. Waser, R. Dittmann, G. Staikov, and K. Szot, Adv. Mater. **21**, 2632 (2009).
[9]C. Lenser, A. Kalinko, A. Kuzmin, D. Berzins, J. Purans, K. Szot, R. Waser, and R. Dittmann, Phys. Chem. Chem. Phys. **13**, 20779 (2011).
[10]C. Lenser, A. Kuzmin, J. Purans, A. Kalinko, R. Waser, and R. Dittmann, J. Appl. Phys. **111**, 076101 (2012).
[11]K. A. Blazey, J. A. Cabrera, and K. A. Müller, Solid State Commun. **45**, 903 (1983).
[12]M. Vračar, A. Kuzmin, R. Merkle, J. Purans, E. A. Kotomin, J. Maier, and O. Mathon, Phys. Rev. B **76**, 174107 (2007).
[13]R. Dovesi, V. R. Saunders, C. Roetti, R. Orlando, C. M. Zicovich-Wilson, F. Pascale, B. Civalleri, K. Doll, N. M. Harrison, I. J. Bush, Ph. D'Arco, and M. Llunell, *CRYSTAL09 User's Manual* (University of Torino, 2009).
[14]R. A. Evarestov, *Quantum Chemistry of Solids* (Springer, Heidelberg, 2007).
[15]J. P. Perdew, M. Ernzerhof, and K. Burke, J. Chem. Phys. **105**, 9982 (1996); M. Ernzerhof and G. E. Scuseria, *ibid.* **110**, 5029 (1999).
[16]M. M. Hurley, L. F. Pacios, P. A. Christiansen, R. B. Ross, and W. C. Ermler, J. Chem. Phys. **84**, 6840 (1986); L. A. LaJohn, P. A. Christiansen, R. B. Ross, T. Atashroo, and W. C. Ermler, *ibid.* **87**, 2812 (1987).
[17]M. Catti, G. Vallerio, and R. Dovesi, Phys. Rev. B **51**, 7441 (1995); R. Krishnan, J. S. Binkley, R. Seeger, and J. A. Pople, J. Chem. Phys. **72**, 650 (1980).
[18]R. A. Evarestov, E. Blokhin, D. Gryaznov, E. A. Kotomin, and J. Maier, Phys. Rev. B **83**, 134108 (2011).
[19]J. J. Rehr and R. C. Albers, Rev. Mod. Phys. **72**, 621 (2000).
[20]A. Bianconi, A. Di Cicco, N. V. Pavel, M. Benfatto, A. Marcelli, C. R. Natoli, P. Pianetta, and J. Woicik, Phys. Rev. B **36**, 6426 (1987).
[21]O. M. Roscioni, P. D'Angelo, G. Chillemi, S. D. Longa, and M. Benfatto, J. Synchrotron. Radiat. **12**, 75 (2005).
[22]Y. Joly, Phys. Rev. B **63**, 125120 (2001).
[23]O. Bunau and Y. Joly, J. Phys.: Condens. Matter **21**, 345501 (2009).
[24]L. Hedin and S. Lundqvist, J. Phys. C **4**, 2064 (1971).
[25]S. E. Dann, D. B. Currie, M. T. Weller, M. F. Thomas, and A. D. Al-Rawwas, J. Solid State Chem. **109**, 134 (1994).
[26]M. T. Buscaglia, V. Buscaglia, M. Viviani, and P. Nanni, J. Am. Ceram. Soc. **84**, 376 (2001).